

Evaluating the Effects of River Partial Penetration on the Occurrence of Riparian Freshwater Lenses

Amir Jazayeri¹, Adrian Deane Werner¹, Huiqiang Wu², and Chunhui Lu²

¹Flinders University

²Hohai University

November 24, 2022

Abstract

Previous studies of freshwater lenses in saline aquifers adjoining gaining rivers (“riparian lenses”) have so far considered only rivers that fully penetrate the aquifer, whereas in most cases, rivers are only partially penetrating. This paper presents a new methodology for obtaining the saltwater discharge and the shape of a steady-state, non-dispersive riparian lens, where the river is partially penetrating, combining two previous analytical solutions. The resulting analytical solution is compared to numerical modelling results to assess assumptions and the methodology adopted to approximate the “turning effect”, which is the change in groundwater flow direction (horizontal to vertical) near the partially penetrating river. A range of conditions are analysed, constrained by parameters adopted previously for River Murray floodplains (Australia). Consistency between analytical and numerical results highlight the capability of the proposed analytical solution to predict the riparian lens geometry and saltwater discharge into partially penetrating rivers. The sensitivity analysis indicates that larger riparian lenses are produced adjacent to the deeper and wider rivers, as expected. The change in width or depth of the river has more influence on the saltwater discharge and the horizontal extent of the riparian lens (and less effect on the vertical extent of the lens adjacent to the river) for shallower and narrower rivers. This research highlights the utility of the new method and demonstrates that the assumption of a fully penetrating river likely leads to significant overestimation of the saltwater discharge to the river and the riparian lens horizontal extent and vertical depth.

Evaluating the Effects of River Partial Penetration on the Occurrence of Riparian Freshwater Lenses

Amir Jazayeri^{1,2}, Adrian D. Werner^{1,2}, Huiqiang Wu^{3,4}, and Chunhui Lu^{3,4}

¹School of the Environment, Flinders University, GPO Box 2100, Adelaide, SA 5001, Australia.

²National Centre for Groundwater Research and Training, Flinders University, GPO Box 2100, Adelaide, SA 5001, Australia.

³State Key Laboratory of Hydrology-Water Resources and Hydraulic Engineering, Hohai University, China.

⁴Yangtze Institute for Conservation and Development, Hohai University, Nanjing, China.

Corresponding author: Amir Jazayeri (amir.jazayeri@flinders.edu.au)

Key Points:

- New method developed to find saltwater discharge and steady-state, non-dispersive riparian lens shape close to a partially penetrating river
- Consistency between analytical and numerical results highlight the capability of proposed methodology.
- Assumption of a fully penetrating river likely leads to significant overestimates of lens size and saltwater discharge to the river.

1 **Abstract**

2 Previous studies of freshwater lenses in saline aquifers adjoining gaining rivers (“riparian
3 lenses”) have so far considered only rivers that fully penetrate the aquifer, whereas in most cases,
4 rivers are only partially penetrating. This paper presents a new methodology for obtaining the
5 saltwater discharge and the shape of a steady-state, non-dispersive riparian lens, where the river is
6 partially penetrating, combining two previous analytical solutions. The resulting analytical
7 solution is compared to numerical modelling results to assess assumptions and the methodology
8 adopted to approximate the “turning effect”, which is the change in groundwater flow direction
9 (horizontal to vertical) near the partially penetrating river. A range of conditions are analysed,
10 constrained by parameters adopted previously for River Murray floodplains (Australia).
11 Consistency between analytical and numerical results highlight the capability of the proposed
12 analytical solution to predict the riparian lens geometry and saltwater discharge into partially
13 penetrating rivers. The sensitivity analysis indicates that larger riparian lenses are produced
14 adjacent to the deeper and wider rivers, as expected. The change in width or depth of the river
15 has more influence on the saltwater discharge and the horizontal extent of the riparian lens (and
16 less effect on the vertical extent of the lens adjacent to the river) for shallower and narrower
17 rivers. This research highlights the utility of the new method and demonstrates that the
18 assumption of a fully penetrating river likely leads to significant overestimation of the saltwater
19 discharge to the river and the riparian lens horizontal extent and vertical depth.

20 **1 Introduction**

21 Buoyant freshwater lenses may occur in riparian zones and within floodplains adjoining
22 freshwater rivers traversing saline aquifers, which are commonly encountered in arid or semi-
23 arid regions (e.g. Cartwright et al., 2010; Cendón et al., 2010; Werner & Laattoe, 2016; Laattoe
24 et al., 2017). These freshwater lenses (i.e. termed “riparian lenses” in this paper) are of great
25 importance in sustaining riparian and floodplain ecosystems, and in the management of river
26 water quality during low-flow periods (e.g. Holland et al., 2009; Telfer et al., 2012). Riparian
27 lenses have been observed under both losing and gaining river conditions. For example,
28 Cartwright et al. (2010), Alaghmand et al. (2014), and Alaghmand et al. (2015) found riparian
29 lenses under losing river conditions in semi-arid floodplains adjacent to the River Murray,
30 Australia. Riparian lenses were encountered by Munday et al. (2006) under gaining river
31 conditions in geophysical surveys conducted in the Bookpurnong floodplain, also adjacent to the
32 River Murray.

33 Werner and Laattoe (2016) showed that gaining-river riparian lenses are caused by
34 buoyancy effects. They derived an analytical solution for the shape of these types of lenses (and
35 for the corresponding saltwater discharge rates) that was verified by Werner et al. (2016) through
36 laboratory experimentation. Werner (2017) subsequently added a correction term to the
37 analytical solution of Werner and Laattoe (2016) to correct for the dispersive mixing that was
38 neglected in assuming of freshwater-saltwater immiscibility.

39 Previous studies of Werner and Laattoe (2016), Werner et al. (2016) and Werner (2017)
40 presumed that the gaining freshwater river penetrates the entire depth of the aquifer. However, it
41 is clear in geological and geophysical-survey cross-sections that the floodplains where riparian
42 lenses were first encountered contain rivers that are incised only partly through the host aquifer
43 (e.g. Munday et al., 2006). The effect of this partial penetration on riparian lenses has not been
44 studied previously.

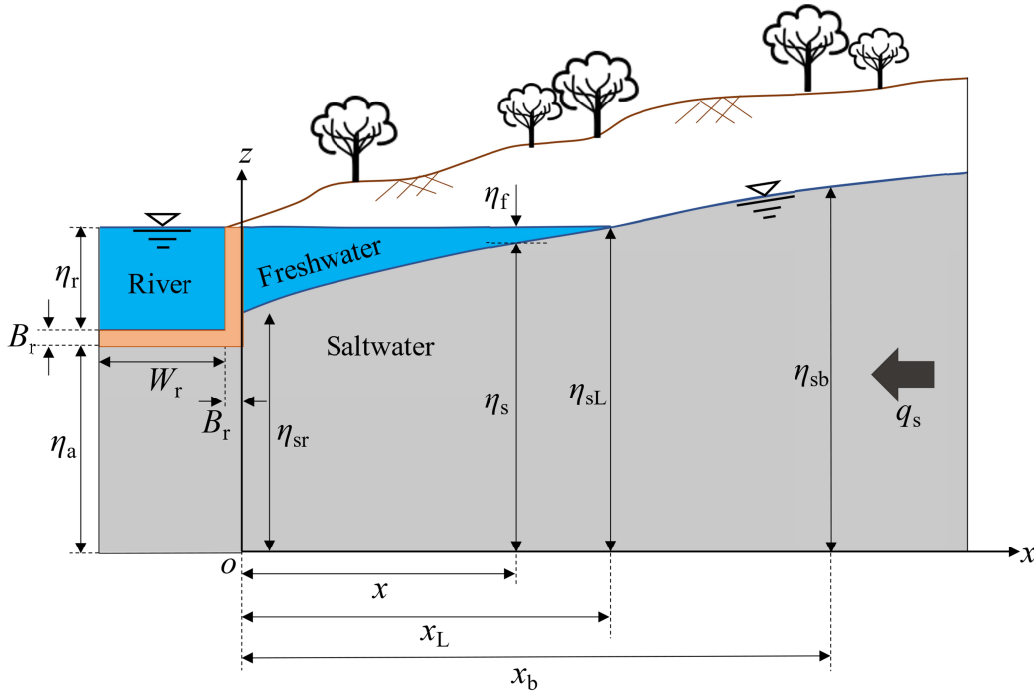
45 Miracapillo and Morel-Seytoux (2014) showed that the depth of river penetration within
 46 an aquifer is an important controlling factor in estimating river-aquifer exchange flow rates.
 47 When a river partially penetrates an aquifer, the direction of groundwater flow to the river
 48 bottom may be effectively vertical, thereby violating the Dupuit-Forchheimer (D-F) assumption
 49 of zero resistance to vertical flow used in earlier methods for calculating river-aquifer
 50 interactions that adopt a fully penetrating river (e.g. Hantush, 1965). To overcome errors
 51 introduced by the change in groundwater flow direction (from horizontal to vertical), Morel-
 52 Seytoux (2009) introduced a “turning factor”, which, simply put, is a factor that modifies the
 53 river-aquifer connectivity that would otherwise apply to a fully penetrating river, thereby
 54 accounting for the resistance caused by the change in flow direction in the vicinity of a partially
 55 penetrating river (a more detailed explanation and mathematical application of the turning factor
 56 is provided later in this article). This followed the earlier work of Morel-Seytoux (1975), who
 57 proposed river loss influence coefficients for incorporating the effect of river penetration. Morel-
 58 Seytoux et al. (2014) provided a table of coefficients (from curve-fitting of analytical values) that
 59 allow for the application of simple formula to obtain the turning factor. They considered the case
 60 of a river placed at the land surface (i.e. does not penetrate the aquifer). Miracapillo and Morel-
 61 Seytoux (2014) modified this approach to account for partial penetration of the aquifer by the
 62 river, and added an approach for calculating the river-aquifer exchange when the heads on the
 63 two sides of the river are different (i.e. asymmetric riparian heads).

64 In this study, the riparian lens theory of Werner and Laattoe (2016) is combined with the
 65 river partial-penetration theory provided by Morel-Seytoux (2009), Miracapillo and Morel-
 66 Seytoux (2014), and Morel-Seytoux et al. (2014) to produce a methodology for estimating
 67 riparian lenses adjacent to partially penetrating rivers that are gaining. This is expected to
 68 broaden the applicability of previous riparian lens solutions that apply only to fully penetrating,
 69 gaining rivers.

70 **2 Theory**

71 This section combines two previous analytical solutions to produce a new methodology
 72 for obtaining the saltwater discharge and the geometry of a steady-state riparian lens adjacent to
 73 a gaining river, which partially penetrates an otherwise saline aquifer. Figure 1 depicts the
 74 corresponding conceptual model, showing the buoyant riparian lens. The riparian lens is
 75 presumed to contain stagnant groundwater, and therefore, the watertable is horizontal. The river
 76 width of $2W_r$ [L] is bisected under the assumption of symmetry. The river penetrates to a depth
 77 η_f [L] into the aquifer and receives steady-state saline groundwater discharge q_s [L^2T^{-1}] (i.e.
 78 discharge per unit length of river perpendicular to the cross-section). Resistive material of
 79 thickness B_r [L] lines the river, and the depth of the aquifer base below the riverbed is η_a [L].
 80 Freshwater and saltwater thicknesses are designated η_f [L] and η_s [L], respectively. The riparian
 81 lens extends to a distance x_L [L] from the origin (point “o”, aligned with the riverbank edge and
 82 the base of the aquifer; Figure 1). Here, at the lens tip, the saltwater thickness is η_{sL} [L]. The
 83 saltwater thickness at the origin (i.e. adjacent to the riverbank) is η_{sr} [L], and η_{sb} is the saltwater
 84 thickness at the landward boundary (or at least the location of a known head or flux of saltwater
 85 towards the river, e.g. from a monitoring well), located at x_b [L].

86



87

88 **Figure 1.** Conceptual model of saline groundwater flow to a partially penetrating river with a
 89 riparian lens adjacent to the river. The river is bisected along an axis of symmetry. Blue and grey
 90 shading represent freshwater and saltwater, respectively.

91

92 Morel-Seytoux (2009) presumed that groundwater flow in an aquifer adjacent to a
 93 partially penetrating river is effectively horizontal at some “far distance” from the river, given
 94 here as x_B [L], whereas closer to the river, the flow has a non-negligible vertical component. The
 95 D-F assumption presumably holds for $x \geq x_B$. Previous studies have presumed that the D-F
 96 assumption applies beyond distances from the river equal to twice the aquifer thickness or
 97 average aquifer thickness (e.g. Haitjema, 1987; Morel-Seytoux, 2009; Morel-Seytoux et al.,
 98 2014, 2017), at least for freshwater-only situations. Applying this notion to the current riparian
 99 lens situation, the value of x_B was taken as $2d_s$, where d_s [L] is the average thickness of saltwater
 100 between the riverbank and at distance x_B . That is:

$$101 \quad d_s = \frac{\eta_{sr} + \eta_{sb}}{2} \quad (1)$$

102 Here, η_{sb} [L] is the saltwater thickness at x_B , and η_{sr} is shown in Figure 1.

103 Flow to the river incorporates the turning factor of Morel-Seytoux (2009). That is, the
 104 exchange flow between the river and aquifer is proportional to the difference in head between the
 105 river and a point in the aquifer sufficiently distant from the river to allow the D-F assumption to
 106 apply (i.e. at $x = x_B$), given for freshwater-only conditions as (Morel-Seytoux, 2009):

$$107 \quad Q = KLG(h_r - h_B) \quad (2)$$

108 where Q [L^3T^{-1}] is the fresh groundwater flow to each side of the river, K [LT^{-1}] is the aquifer
 109 hydraulic conductivity (in this case, for freshwater), L [L] is the river reach length (perpendicular
 110 to the river cross-section), Γ [-] is the one-side dimensionless conductance, h_r [L] is the head in
 111 the river, and h_B [L] is the head in the aquifer at x_B .

112 Equation (2) needs modification to apply to the conceptual model of Figure 1 because of
 113 the effects on flow of having two fluids (freshwater and saltwater) of different densities. To
 114 account for saltwater flow beneath a buoyant riparian lens, equation (2) is modified to express
 115 head variables in equivalent saltwater head terms, in a similar manner to Werner and Laattoe
 116 (2016), as:

$$117 \quad q_s = K_s \Gamma_s (h_{sr} - h_{sB}) \quad (3)$$

118 Here, L in equation (2) is taken as unity, reducing Q to q_s . K_s [LT^{-1}] is the saltwater hydraulic
 119 conductivity of the aquifer, which relates to the freshwater K through $K_s = \rho_s \mu_f K / (\rho_f \mu_s)$, where ρ_s
 120 and ρ_f are saltwater and freshwater densities [ML^{-3}] and μ_s and μ_f are freshwater and saltwater
 121 dynamic viscosities [$ML^{-1}T^{-1}$], respectively. For simplicity, $\mu_f / \mu_s = 1$ is adopted. Γ_s [-] is the
 122 modified, one-side, dimensionless conductance for saltwater flow, which is defined in Section
 123 2.3. h_{sr} and h_{sB} [L] are equivalent hydrostatic saltwater heads at the river and at x_B , respectively.
 124 The former is given by:

$$125 \quad h_{sr} = \eta_a + B_r + \frac{\rho_f}{\rho_s} \eta_r \quad (4)$$

126 h_{sB} depends on whether x_B is beyond or within the extent of the riparian lens, as discussed in
 127 subsections that follow.

128 2.1 Scenario 1: x_B within the riparian lens area ($x_B < x_L$)

129 Where the riparian lens exists ($x \leq x_L$; Figure 1), the combined thickness of the lens and
 130 underlying saltwater is equal to the height of the river water level above the aquifer base,
 131 namely:

$$132 \quad \eta_s + \eta_f = \eta_{sL} = \eta_a + B_r + \eta_r \quad (5)$$

133 Within the area of the lens where the D-F assumption is valid ($x_B \leq x \leq x_L$), the saltwater
 134 head that drives (saltwater) flow is equal to the depth of saltwater flow (η_s) plus the saltwater
 135 head caused by the (freshwater) riparian lens, giving rise to an equivalent saltwater head (h_s [L])
 136 of:

$$137 \quad h_s = \eta_s + \frac{\rho_f}{\rho_s} \eta_f \quad (6)$$

138 Combining equations (5) and (6) produces:

$$139 \quad h_s = \eta_s + \frac{\rho_f}{\rho_s} (\eta_a + B_r + \eta_r - \eta_s) \quad (7)$$

140 Noting that at x_B , $h_s = h_{sB}$, and $\eta_s = \eta_{sB}$, and combining equations (3), (4) and (7) leads to:

$$141 \quad q_s = K_s \Gamma_s \left(1 - \frac{\rho_f}{\rho_s} \right) (\eta_a + B_r - \eta_{sB}) \quad (8a)$$

142 And:

$$143 \quad \eta_{sB} = \eta_a + B_r - \frac{q_s}{K_s \Gamma_s \left(1 - \frac{\rho_f}{\rho_s} \right)} \quad (8b)$$

144 Where the D-F assumption is applicable ($x \geq x_B$), saltwater flow (i.e. q_s) can be described
145 by Darcy's law for horizontal flow:

$$146 \quad q_s = -K_s \eta_s \frac{dh_s}{dx} \quad (9)$$

147 Beyond the extent of the lens ($x \geq x_L$), q_s is given by:

$$148 \quad q_s = -K_s \eta_s \frac{d\eta_s}{dx} \quad (10)$$

149 By taking the definite integration of equation (10) between two arbitrary points, x_1 and x_2 ,
150 where $x_L \leq x_1, x_2 \leq x_b$, then:

$$151 \quad q_s (x_2 - x_1) = -\frac{K_s}{2} (\eta_{s2}^2 - \eta_{s1}^2) \quad (11)$$

152 Substituting $x_1 = x_L, \eta_{s1} = \eta_{sL}, x_2 = x_b$ and $\eta_{s2} = \eta_{sb}$ into equation (11), q_s can be found as:

$$153 \quad q_s = -\frac{K_s}{2(x_b - x_L)} (\eta_{sb}^2 - \eta_{sL}^2) \quad (12a)$$

154 And:

$$155 \quad x_L = \frac{K_s}{2q_s} (\eta_{sb}^2 - \eta_{sL}^2) + x_b \quad (12b)$$

156 The equation for saltwater flow beneath the lens, for region $x \geq x_B$, can be obtained by
157 substituting equation (7) into equation (9), producing (Werner & Laattoe, 2016):

$$158 \quad q_s = -K_s \left(1 - \frac{\rho_f}{\rho_s} \right) \eta_s \frac{d\eta_s}{dx} \quad (13)$$

159 The definite integral of equation (13), between x_1 and x_2 , where $x_B \leq x_1, x_2 \leq x_L$ becomes:

$$160 \quad q_s (x_2 - x_1) = -\frac{K_s}{2} \left(1 - \frac{\rho_f}{\rho_s} \right) (\eta_{s2}^2 - \eta_{s1}^2) \quad (14)$$

161 Substituting $x_1 = x_B, \eta_{s1} = \eta_{sB}, x_2 = x_L$ and $\eta_{s2} = \eta_{sL}$, equation (14) becomes:

$$q_s = -\frac{K_s}{2(x_L - x_B)} \left(1 - \frac{\rho_f}{\rho_s}\right) (\eta_{sL}^2 - \eta_{sB}^2) \quad (15)$$

Seeking q_s as a function of variables that can be measured in field situations, we eliminate η_{sB} and x_L by combining equations (8b), (12b) and (15), resulting in the following quadratic equation:

$$aq_s^2 + bq_s + c = 0 \quad (16)$$

where coefficients a , b and c are given by:

$$a = -\frac{1}{K_s \Gamma_s^2 \left(1 - \frac{\rho_f}{\rho_s}\right)} \quad (17a)$$

$$b = 2 \left(x_b - x_B + \frac{(\eta_a + B_r)}{\Gamma_s} \right) \quad (17b)$$

$$c = K_s \left(\eta_{sB}^2 - \frac{\rho_f}{\rho_s} \eta_{sL}^2 - \left(1 - \frac{\rho_f}{\rho_s}\right) (\eta_a + B_r)^2 \right) \quad (17c)$$

Equation (16) can easily be solved to obtain q_s , and the lens extent, x_L is then attainable from equation (12b).

2.2 Scenario 2: x_B outside the riparian lens area ($x_B > x_L$)

When x_B is located outside the riparian lens area, the saltwater head at x_B is equal to the saltwater thickness (i.e. $h_{sB} = \eta_{sB}$), which in combination with equations (3) and (4) produces:

$$q_s = K_s \Gamma_s \left(\eta_a + B_r + \frac{\rho_f}{\rho_s} \eta_r - \eta_{sB} \right) \quad (18a)$$

And:

$$\eta_{sB} = \eta_a + B_r + \frac{\rho_f}{\rho_s} \eta_r - \frac{q_s}{K_s \Gamma_s} \quad (18b)$$

In addition, in the saltwater region, by substituting $x_1 = x_B$, $\eta_{s1} = \eta_{sB}$, $x_2 = x_b$ and $\eta_{s2} = \eta_{sL}$ into equation (11), q_s can be obtained as:

$$q_s = -\frac{K_s}{2(x_b - x_B)} (\eta_{sB}^2 - \eta_{sL}^2) \quad (19)$$

Substituting equation (18b) into equation (19) leads again to a quadratic expression in the form of equation (16), where coefficients a , b and c are given by:

$$a = \left(\frac{1}{K_s \Gamma_s} \right)^2 \quad (20a)$$

$$b = \frac{-2}{K_s} \left(x_b - x_B + \frac{\left(\eta_a + B_r + \frac{\rho_f}{\rho_s} \eta_r \right)}{\Gamma_s} \right) \quad (20b)$$

$$c = \left(\eta_a + B_r + \frac{\rho_f}{\rho_s} \eta_r \right)^2 - \eta_{sb}^2 \quad (20c)$$

187 The value of q_s can again be achieved by solving equation (16), allowing x_L to be
 188 obtained from equation (12b).

189 2.3 Modified, one-side, dimensionless conductance for saltwater flow to the river (Γ_s)

190 Morel-Seytoux (2009) showed, for freshwater-only problems, that Γ is a function of the
 191 normalized wetted perimeter, W_p^N [-], and the normalised degree of penetration, d_p^N [-] of the
 192 river. W_p^N is W_p/d , where W_p is the wetted perimeter of the river and d is the average aquifer
 193 thickness, or simply the aquifer thickness. d_p^N is η_r/d . Modification of the method for obtaining Γ
 194 is required to account for the buoyant riparian lens. That is, W_p^N is replaced with a saltwater
 195 normalised wetted perimeter (W_{sp}^N [-]), which we define as:

$$W_{sp}^N = \frac{W_{sp}}{d_s} = \frac{2(W_r + (\eta_{sr} - \eta_a - B_r))}{d_s} \quad (21)$$

197 where W_{sp} is the total wetted perimeter through which saltwater discharges (on both sides of the
 198 river). d_p^N is replaced with a saltwater normalised degree of penetration (d_{sp}^N [-]), given by:

$$d_{sp}^N = \frac{\eta_{sr} - \eta_a - B_r}{d_s} \quad (22)$$

200 By using W_{sp}^N and d_{sp}^N obtained from equations (21) and (22), instead of W_p^N and d_p^N for
 201 freshwater-only situations, Γ_s can be calculated by the following steps. Firstly, the value of Γ_s for
 202 the situation of no river penetration or a flat recharge zone (i.e. Γ_{flat} [-]) is calculated from
 203 (Morel-Seytoux et al., 2014):

$$\Gamma_{flat} = \frac{1}{2 \left[1 + \frac{1}{\pi} \ln \left(\frac{2}{1 - \sqrt{e^{-\pi W_{sp}^N}}} \right) \right]} \quad (23)$$

205 Secondly, Γ_{flat} is adjusted to account for partial penetration of the river (Miracapillo &
 206 Morel-Seytoux, 2014):

$$\Gamma_p = \Gamma_{flat} \left[1 + a_1 d_{sp}^N + a_2 (d_{sp}^N)^2 \right] \quad (24)$$

208 where a_1 [-] and a_2 [-] are given in Table 1.

209

210 **Table 1.** Values for partial penetration coefficients in equation (24), given by Morel-Seytoux et
211 al. (2014).

W_{sp}^N range	d_{sp}^N range	a_1	a_2
$W_{sp}^N \leq 1.0$	$d_{sp}^N \leq 0.2$	0.890	-2.430
$W_{sp}^N \leq 1.0$	$0.2 < d_{sp}^N \leq 0.5$	0.538	-0.387
$1.0 < W_{sp}^N \leq 3.0$	$d_{sp}^N \leq 0.2$	0.819	-1.340
$1.0 < W_{sp}^N \leq 3.0$	$0.2 < d_{sp}^N \leq 0.5$	0.672	-0.542
$1.0 < W_{sp}^N \leq 3.0$	$0.5 < d_{sp}^N \leq 0.9$	0.567	-0.330

212

213 Finally, a modification to the conductance is required if a clogging layer exists (Morel-
214 Seytoux, 2009):

$$215 \quad \Gamma_c = \frac{\Gamma_p}{\left(1 + 2 \left(\frac{B_r}{W_{sp}}\right) \left(\frac{K_s}{K_{sc}}\right) \Gamma_p\right)} \quad (25)$$

216 Here, K_{sc} [LT^{-1}] is the saltwater hydraulic conductivity of the clogging layer. Thus, Γ_s is either Γ_p
217 or Γ_c depending on the existence of a clogging layer.

218 2.4 Applying the analytical solution

219 Calculating q_s using the analytical solution obtained in this study requires knowledge of
220 the position of x_B relative to x_L , which is dependent on q_s via equation (12b), and q_s is
221 determinable from knowledge of the boundary conditions and other measurable parameters
222 according to equations (16) and (17a-c) or (20a-c) (the choice of which depends on the position
223 of x_B relative to x_L). Hence, solving for q_s and x_L requires iteration of the theory given earlier.

224 Several assumptions were used to approximate the initial values required to start the
225 iteration process. Firstly, $d_s \approx \eta_a$ (and hence $x_B \approx 2\eta_a$) was adopted. Secondly, the values of W_{sp}^N
226 and d_{sp}^N required to calculate Γ_s were approximated by $W_{sp} \approx 2W_r$ (i.e. assuming that $(\eta_{sr} - \eta_a -$
227 $B_r) \ll W_r$), and the equivalent saltwater depth within the river (i.e. $\eta_r \rho_f / \rho_s$) was chosen as a
228 replacement for $(\eta_{sr} - \eta_a - B_r)$ in equation (22), leading to the following initial estimates:

$$229 \quad W_{sp}^N \approx \frac{2W_r}{\eta_a} \quad (26)$$

230
$$d_{sp}^N \approx \frac{(\rho_f / \rho_s) \eta_r}{\eta_a} \quad (27)$$

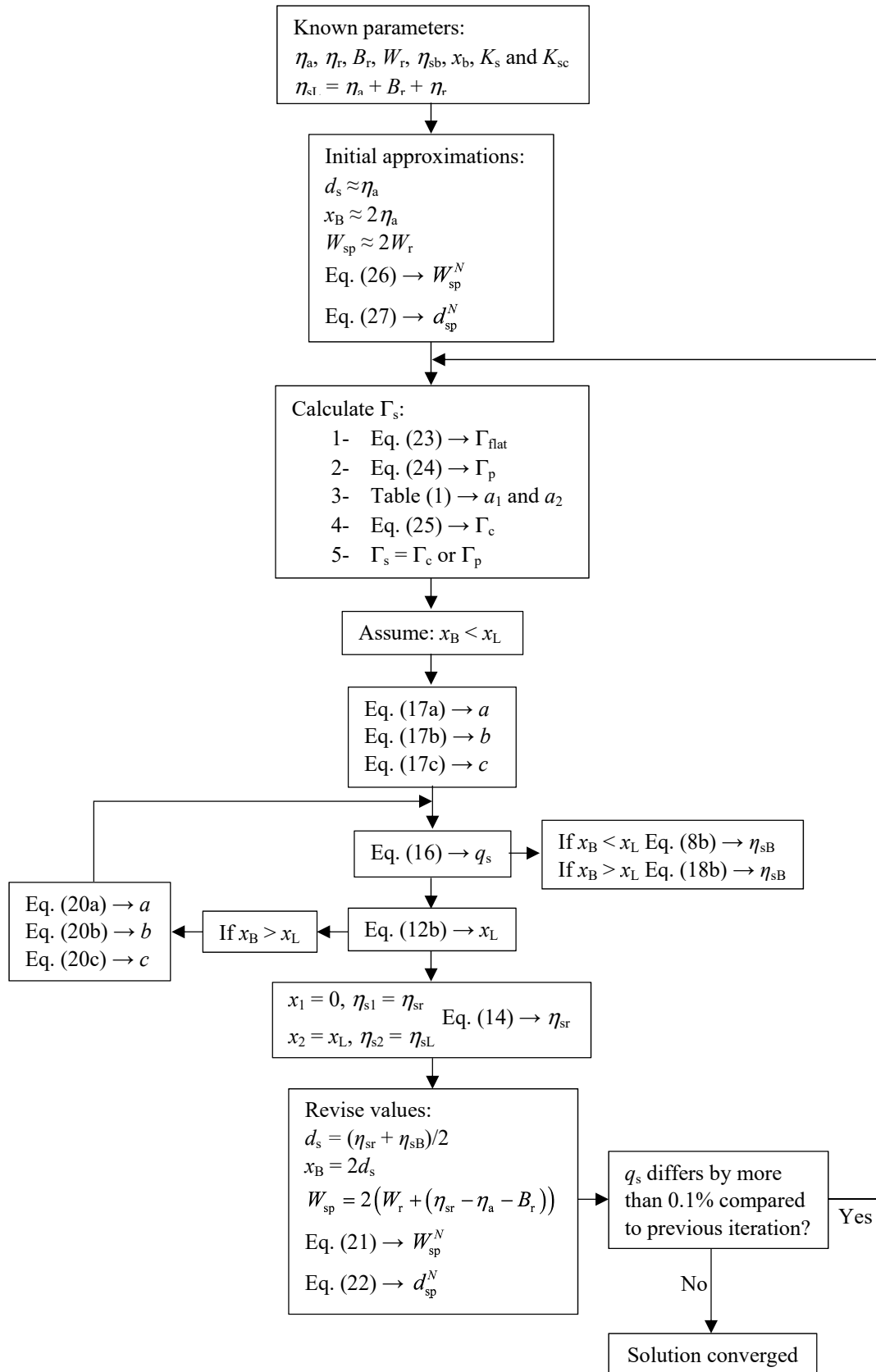
231 Using equations (26) and (27), the initial value of Γ_s can be calculated from equations
 232 (23) to (25). Thirdly, it was assumed that $x_B < x_L$, and therefore the initial value of Γ_s is used in
 233 equations (17a-c) to find the coefficients in equation (16). Note that the solution to equation (16)
 234 to find q_s has two roots, only one of which is acceptable; namely the negative root indicating
 235 saltwater flow towards the river.

236 The value of q_s is then applied in equation (12b) to calculate x_L . The value of x_L is
 237 compared with x_B to check if the initial assumption of $x_B < x_L$ was correct or not. If $x_B > x_L$,
 238 equations (20a-c) should be used to calculate the coefficients of equation (16). The new value of
 239 q_s can be obtained by finding the negative root of equation (16), which is used in equation (12b)
 240 to find a new value for x_L . The obtained values of q_s and x_L can be used to find η_{sB} through
 241 application of equation (8b) (if $x_B < x_L$) or equation (18b) (if $x_B > x_L$). Values of q_s and x_L also
 242 allow for the calculation of η_{sr} using equation (14) (by substituting $x_1 = 0$, $\eta_{s1} = \eta_{sr}$, $x_2 = x_L$ and
 243 $\eta_{s2} = \eta_{sL}$). The corrected values of variables d_s , x_B , W_{sp} , W_{sp}^N and d_{sp}^N can be calculated from the
 244 obtained values of η_{sr} and η_{sB} through equation (1) (to find d_s), equation (21) (to find W_{sp}^N) and
 245 equation (22) (to find d_{sp}^N). Then, the above method is repeated to find new values of Γ_s , q_s , x_L ,
 246 η_{sr} and η_{sB} . The iteration procedure needs to be continued until convergence criteria are met. We
 247 ceased iterating once the change in q_s between two consecutive iterations was less than 0.1%.

248 After finding the converged values of q_s and x_L , the freshwater-saltwater interface can be tracked
 249 using equation (14) by adopting $x_1 = x$, $\eta_{s1} = \eta_s$, $x_2 = x_L$ and $\eta_{s2} = \eta_{sL}$, as:

250
$$\eta_s = \sqrt{\frac{2q_s(x_L - x)}{K_s \left(1 - \frac{\rho_f}{\rho_s}\right)} + \eta_{sL}}^2 \quad (28)$$

251 The iteration procedure required to apply the above analytical solution is summarised as a
 252 flowchart in Figure 2.



254 **Figure 2.** Flowchart of iteration method for applying the partially penetrating riparian
 255 lens analytical solution (“Eq.” means “Equation”).

256

257 It should be noted that equation (28) is based on the D-F assumption, which is presumed
 258 to hold for the region $x_B \leq x \leq x_L$. For the region $0 \leq x < x_B$, where a component of vertical flow
 259 is expected, equation (28) is also used to deduce the lens shape, including η_{sr} , in the absence of
 260 an alternative formula for the lens shape in this near-river region. This introduces some errors in
 261 the analytical solution for the near-river part of the lens ($0 \leq x < x_B$) that are assessed in Section
 262 3. Even though lens calculations for $0 \leq x < x_B$ do not comply with the D-F assumption, any error
 263 associated with that non-compliance does not necessarily influence other calculations within the
 264 analytical approach (e.g. calculated values of x_L and q_s).

265 **3 Comparison to numerical modelling**

266 3.1 Description of model setup

267 Numerical modelling of partially penetrating rivers lined with low- K streambed material
 268 was undertaken using SEAWAT (version 4; Langevin et al., 2008) to evaluate the analytical
 269 solution proposed herein. SEAWAT has been extensively used and validated for variable-density
 270 flow and solute transport, combining MODFLOW-2000 (Harbaugh et al., 2000) and MT3DMS
 271 (Zheng & Wang, 1999) through the water density term. For brevity, the mathematical
 272 formulation of SEAWAT is not shown here and the reader is referred to the software
 273 documentation (Guo & Langevin, 2002).

274 Various river geometries (width and depth of penetration) were tested using cross-
 275 sectional simulations of an unconfined aquifer. The vertical extent of the numerical model
 276 domain for all cases was constant at 10 m, while the horizontal extent was varied from 95 to 99
 277 m to obtain the same distance between the riverbank edge and the landward boundary (i.e. 90 m),
 278 despite different W_r . The numerical models adopt the cell widths ranging from 0.19 to 0.198 m
 279 and a depth of 0.2 m, leading to a total of 25,000 cells. This achieved a balance between
 280 accuracy of the results and reasonable computational run times, which were up to one hour on a
 281 quadcore Intel® Core™ i5-7500 processor.

282 The saltwater boundary was represented by specified-head boundary condition, while the
 283 freshwater river was simulated using the General-Head Boundary (GHB) package of SEAWAT
 284 (Langevin et al., 2008). Use of the GHB package allowed flow into or out of the model domain
 285 (via the river) depending on the resistance of a clogging layer, represented by the boundary
 286 conductance. Specifically, following the guidance given in (Harbaugh et al., 2000) the GHB
 287 conductance (C_{GHB} [L^2T^{-1}]) was set to:

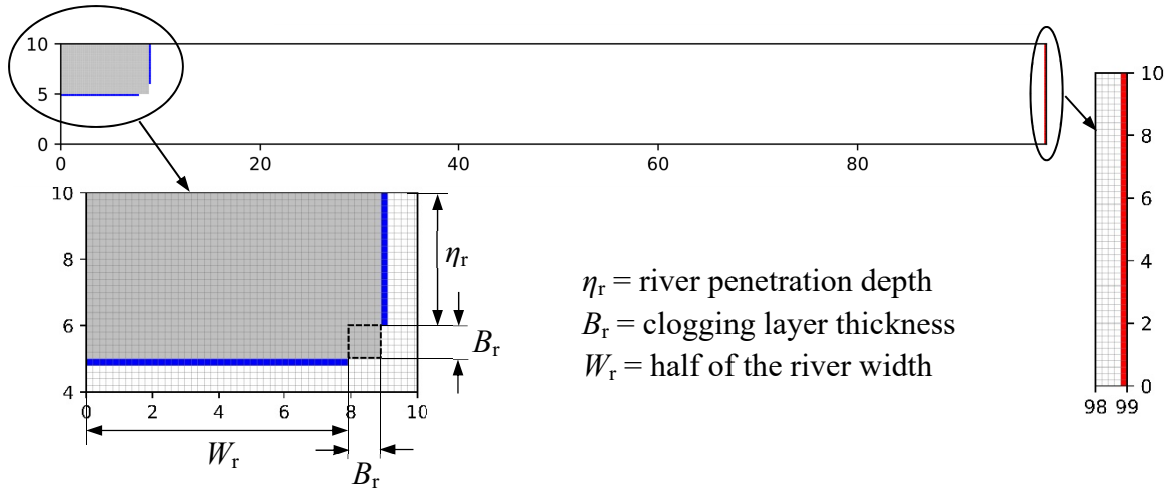
$$288 \quad C_{GHB} = \frac{KK_c \Delta A}{\left(KB_r + K_c \frac{\Delta L}{2} \right)} \quad (29)$$

289 where ΔA [L^2] is the cell cross-sectional area perpendicular to the flow. For horizontal GHB cells
 290 along the horizontal river bottom, $\Delta A = \Delta x \Delta y$ and for the vertical riverbank, $\Delta A = \Delta z \Delta y$, where
 291 Δx , Δz and Δy (Δy is perpendicular to the river cross-section and is equal to 1 m) are the cell size
 292 [L] in x , z and y (perpendicular to the river cross-section) directions, respectively. ΔL [L] is the

293 cell size in the direction of flow (i.e. Δz and Δx for GHB cells representing the parts of the river
 294 boundary that are horizontal and vertical, respectively).

295 Figure 3 illustrates an example of the model boundary conditions and river geometry,
 296 representing Case E-4 in the current study.

297



298

299 **Figure 3.** An example of model domain (for Case E-4; described in Table 3). Red, blue and grey
 300 cells represent specified-head (saltwater; solute concentration = 1), general-head (freshwater;
 301 solute concentration = 0) and no-flow (inactive) boundary conditions, respectively. The black
 302 dashed lines in the lower right corner of the incised area where, conceptually, the clogging layer
 303 does not abut river water. A more detailed explanation for the lack of GHB boundary cells (blue)
 304 along the lower-right corner of the inactive zone is offered in the main text. Units are in metres.

305

306 Figure 3 shows that GHB boundary cells are not used to represent the entire perimeter of
 307 the incised area in the top left corner of the model, which represents the physical space occupied
 308 by the river and surrounding riverbed materials. This is because the GHB boundary cells
 309 represent the connection of the aquifer to the river through riverbed material. The GHB cells
 310 simulate river-aquifer connection that occurs perpendicular to the riverbed (horizontal river
 311 bottom) and the riverbank (vertical side of the river). Therefore, as the clogging layer in the
 312 lower right corner of the incised region does not connect the aquifer to water river (perpendicular
 313 to the boundary), we omitted any connectivity between the aquifer and the river along the outer
 314 edge of these cells (i.e. there are no GHB cells along this part of the perimeter). An alternative to
 315 this approach could have been to try to parameterise GHB cells in this region considering the
 316 convergent flow that might occur through the corner square of riverbed material, i.e., towards the
 317 lower right corner of the river. This would have required a rather arbitrary choice of conductance
 318 (which would have been lower than the value used along other parts of the boundary where flow
 319 to the river is perpendicular to the riverbank/riverbed), so we prefer simply to disconnect the
 320 aquifer from the river where there is not a connection to the aquifer in the direction perpendicular
 321 to the river boundary. This resulted in vertical and horizontal lengths of the incised region equal
 322 to B_r where no GHB cells were placed (i.e. the square region shown by black dashed lines in
 323 Figure 3), while GHB cells covered a horizontal distance of W_r and a vertical distance of η_r ,

324 corresponding with the river width and depth, respectively. Also, preliminary model testing
 325 found that a better match to the analytical solution was obtained with the approach to GHB cell
 326 distribution in Figure 3.

327 Solute concentrations at specified-head and general-head boundaries were dealt with in
 328 the Sink and Source Mixing (SSM) package of MT3DMS (Zheng & Wang, 1999). This allowed
 329 groundwater discharge to occur at the ambient salt concentration, and incoming groundwater to
 330 have specified salinity levels (e.g. freshwater in the case of the river and saltwater at the inland
 331 boundary). The SEAWAT models were run in transient mode until steady-state conditions were
 332 achieved, as indicated by time-invariant total solute mass in the model. Periods needed to reach
 333 steady-state conditions were in the order of 5000 to 8000 days.

334 The parameters adopted in numerical models (and corresponding analytical solutions,
 335 where parameters are relevant) were chosen to be consistent with previous studies (e.g. Werner,
 336 2017) and are considered reasonable for River Murray conditions (i.e. consistent with parameter
 337 ranges provided by Werner and Laattoe (2016) for typical River Murray conditions). Parameter
 338 values are given in Table 2.

339

340 **Table 2.** Parameters used in numerical and analytical models.

Parameter	Symbol	Value	Unit
Aquifer freshwater hydraulic conductivity ^a	K	10	m/d
Clogging layer freshwater hydraulic conductivity ^a	K_c	1	m/d
Clogging layer thickness	B_r	1	m
Freshwater density	ρ_f	1000	kg/m ³
Saltwater density	ρ_s	1025	kg/m ³
Distance of landward boundary from riverbank	x_b	90	m
Saltwater thickness at landward boundary	η_{sb}	10.05	m
Specific yield ^b	S_y	0.24	–
Specific storage ^b	S_s	10^{-6}	1/m
Effective porosity ^b	n	0.3	–

341 ^aSEAWAT uses K and K_c as input, while K_s and K_{sc} should be adopted in the analytical solution.

342 ^bParameter used only in numerical models.

343

344 Dispersion parameters in numerical models (i.e. longitudinal dispersivity, α_L [L],
 345 transverse dispersivity, α_T [L], and molecular diffusion, D_m [L²T⁻¹]) were set to zero as an
 346 attempt to simulate non-dispersive, sharp-interface conditions (or at least minimal dispersion).
 347 However, some dispersion occurred in SEAWAT due to unavoidable artificial numerical
 348 dispersion (Werner, 2017).

349 Twenty cases were used to consider various river geometries, including river widths and
 350 depths varying from 4 to 8 m and 1 to 4 m, respectively. These river geometries correspond to

351 W_{sp}^N and d_{sp}^N ranging from 0.95 to 2.40 and 0.05 to 0.15, respectively. Table 3 provides the
 352 parameters for various river geometries used in analytical and numerical models.

353

354 **Table 3.** Parameters for various river geometries adopted in numerical and analytical models.

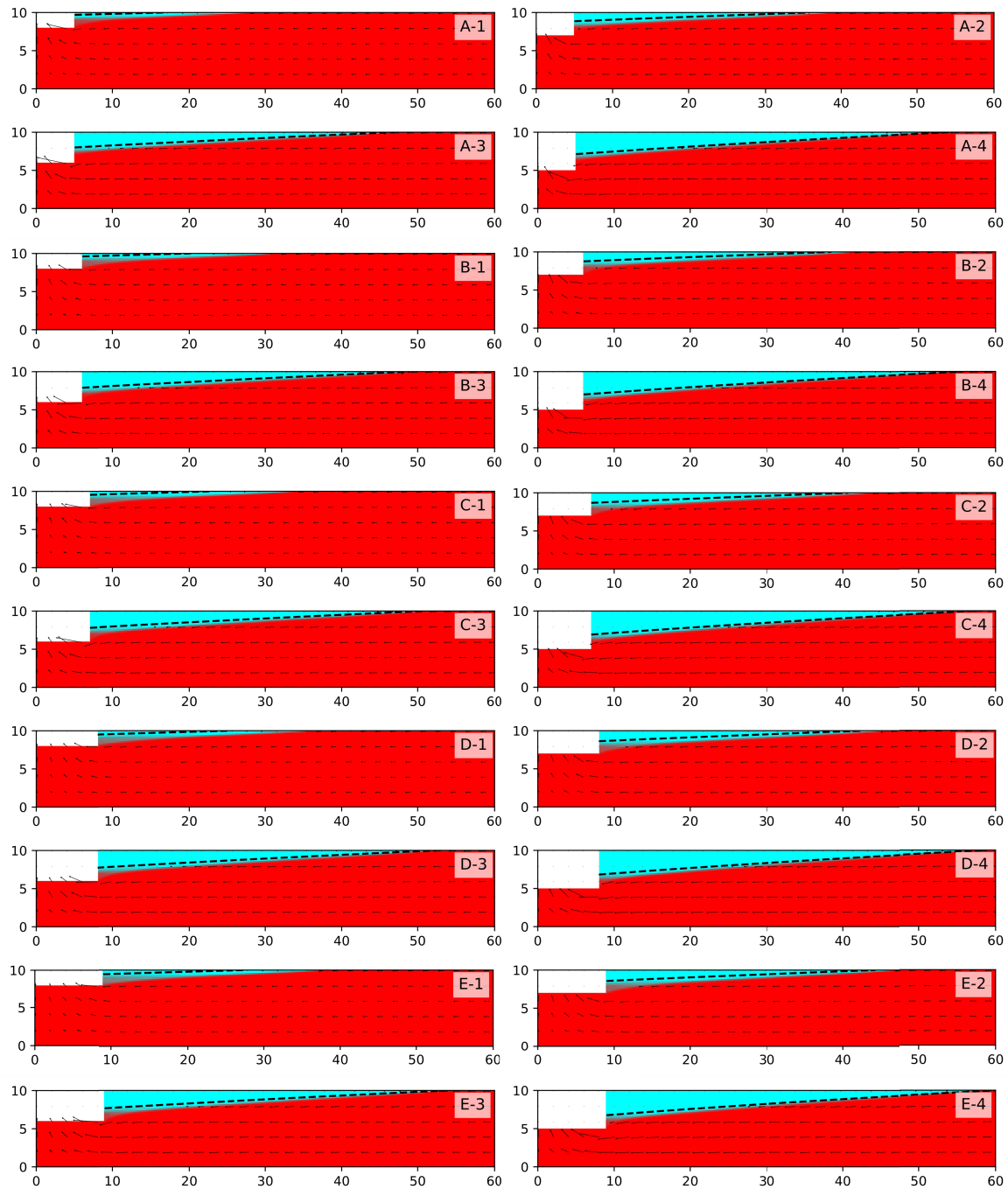
River depth	η_r (m)	1	2	3	4	
Depth of aquifer beneath riverbed base	η_a (m)	8	7	6	5	
River half-width	W_r (m)	4	A-1	A-2	A-3	A-4
		5	B-1	B-2	B-3	B-4
		6	C-1	C-2	C-3	C-4
		7	D-1	D-2	D-3	D-4
		8	E-1	E-2	E-3	E-4

355

356 3.2 Analytical solution and numerical simulation results and comparison

357 The steady-state salinity distributions of numerical models and the sharp-interface of the
 358 analytical solution for various river geometries are shown in Figure 4, with key results listed in
 359 Table 4, which also contains the discrepancies in the three main riparian lens characteristics (i.e.
 360 q_s , x_L and η_{sr}). Here, numerical results for x_L and η_{sr} are compared to the analytical solution by
 361 considering the 0.5 relative salinity concentration (i.e. 50% saltwater concentrations) isochlor
 362 from numerical models.

363



364

365 **Figure 4.** Comparison between numerical model salinity distributions (cyan and red are
 366 freshwater and saltwater, respectively) and sharp-interface tracked line (black dashed line) from
 367 analytical solution. Arrows indicate the velocity vectors from numerical simulations (one in ten
 368 vectors is shown). An explanation of each case is given in Table 3. Units are in metres and
 369 salinity varies from 0 (freshwater) to 1 (saltwater). Note that only a portion of the model domain
 370 (60 m from the river centre) is shown for clarity.

371

372

Table 4. Numerical and analytical model results of q_s , x_L and η_{sr} for different cases.

Case	Numerical model ^a			Analytical solution			Difference ^b (%)		
	q_s (m ² /s)	x_L (m)	η_{sr} (m)	q_s (m ² /s)	x_L (m)	η_{sr} (m)	q_s	x_L	η_{sr}
A-1	-0.0834	23.10	9.10	-0.0656	11.69	9.69	-21.3	-49.4	6.43
A-2	-0.102	35.03	8.27	-0.0869	30.89	8.86	-14.7	-11.8	7.21
A-3	-0.119	42.63	7.48	-0.107	41.94	8.01	-10.3	-1.61	7.10
A-4	-0.135	47.98	6.69	-0.125	49.01	7.13	-7.14	2.16	6.66
B-1	-0.0868	25.24	9.01	-0.0678	14.21	9.61	-21.9	-43.7	6.60
B-2	-0.106	36.60	8.12	-0.0894	32.50	8.76	-15.3	-11.2	7.87
B-3	-0.123	43.91	7.30	-0.109	43.05	7.89	-10.9	-1.96	8.08
B-4	-0.138	49.00	6.50	-0.128	49.81	7.00	-7.64	1.65	7.78
C-1	-0.0892	27.03	8.87	-0.0695	16.03	9.54	-22.2	-40.7	7.63
C-2	-0.108	37.70	8.02	-0.0912	33.69	8.68	-15.6	-10.7	8.29
C-3	-0.125	44.81	7.18	-0.111	43.87	7.80	-11.2	-2.09	8.68
C-4	-0.141	49.69	6.37	-0.130	50.40	6.91	-7.89	1.43	8.46
D-1	-0.0910	28.45	8.70	-0.0708	17.40	9.49	-22.3	-38.9	9.08
D-2	-0.110	38.44	7.94	-0.0927	34.58	8.62	-15.8	-10.0	8.63
D-3	-0.127	45.40	7.09	-0.113	44.50	7.73	-11.3	-1.98	9.04
D-4	-0.143	50.14	6.27	-0.131	50.86	6.83	-7.96	1.44	8.85
E-1	-0.0920	32.31	8.45	-0.0718	18.45	9.46	-22.0	-42.9	11.9
E-2	-0.111	38.88	7.89	-0.0939	35.27	8.57	-15.5	-9.28	8.64
E-3	-0.128	45.70	7.04	-0.114	45.00	7.67	-11.0	-1.55	9.04
E-4	-0.144	50.40	6.22	-0.133	51.22	6.76	-7.65	1.62	8.65

373

^aBased on 0.5 relative salinity concentration (i.e. 50‰ saltwater concentrations) isochlor.

374

^b(analytical result – numerical result)/numerical result × 100%.

375

376

377

378

379

380

381

382

383

384

The numerical and analytical results given in Figure 4 and Table 4 indicate that shallow rivers produce much smaller riparian lenses than those adjacent to rivers that penetrate almost the entire aquifer thickness, thus highlighting the benefit of the partially penetrating solution. The proposed analytical solution provides a reasonable prediction of the riparian lens geometry and saltwater discharge into partially penetrating rivers for the majority of cases. For example, differences between numerical simulations and analytical results has a maximum of 22% for q_s , which was obtained for the case of the smallest river penetration depth (i.e. $\eta_r = 1$ m; Cases A-1, B-1, C-1, D-1 and E-1). In other cases, q_s discrepancies are less than 16%. Table 4 shows that the analytical solution tends to underestimate the magnitude of q_s in all cases.

385 In terms of x_L , the analytical solution and numerical models differ by less than 12% for
 386 all cases except those with river depths of 1 m (i.e. Cases A-1, B-1, C-1, D-1 and E-1), for which
 387 significant analytical-numerical discrepancies were obtained (39-49%). We attribute these high
 388 errors to the stronger vertical flows that arise in the cases with the shallowest rivers (i.e. smallest
 389 η_r of 1 m), leading to the largest departures from the D-F assumption adopted in the analytical
 390 solution. Lens extents were underestimated by the analytical solution, relative to numerical
 391 results, in 15 of the 20 cases listed in Table 4.

392 Analytical-numerical differences in η_{sr} were less than 12% in all cases, and were
 393 overestimated by the analytical solution. Therefore, riparian lenses obtained using the new
 394 method are deeper but extend a shorter distance from the riverbank compared to those from
 395 numerical models.

396 Statistical criteria, including mean absolute error (MAE), root mean square error
 397 (RMSE), percent bias (PBIAS) and Nash-Sutcliffe efficiency (NSE) (Moriassi et al., 2007), are
 398 presented in Table 5 to evaluate the match between analytical solution and numerical
 399 simulations. MAE, RMSE, PBIAS values closer to 0 and NSE closer to 1 indicate better
 400 agreement (Moriassi et al., 2007). The sign of PBIAS values in Table 5 indicate that the analytical
 401 solution underestimates both q_s and x_L , while η_{sr} was overestimated (as described above). These
 402 statistics considered together suggest that the analytical and numerical models are generally in
 403 reasonable agreement.

404

405 **Table 5.** Statistical criteria to evaluate analytical-numerical model agreement.

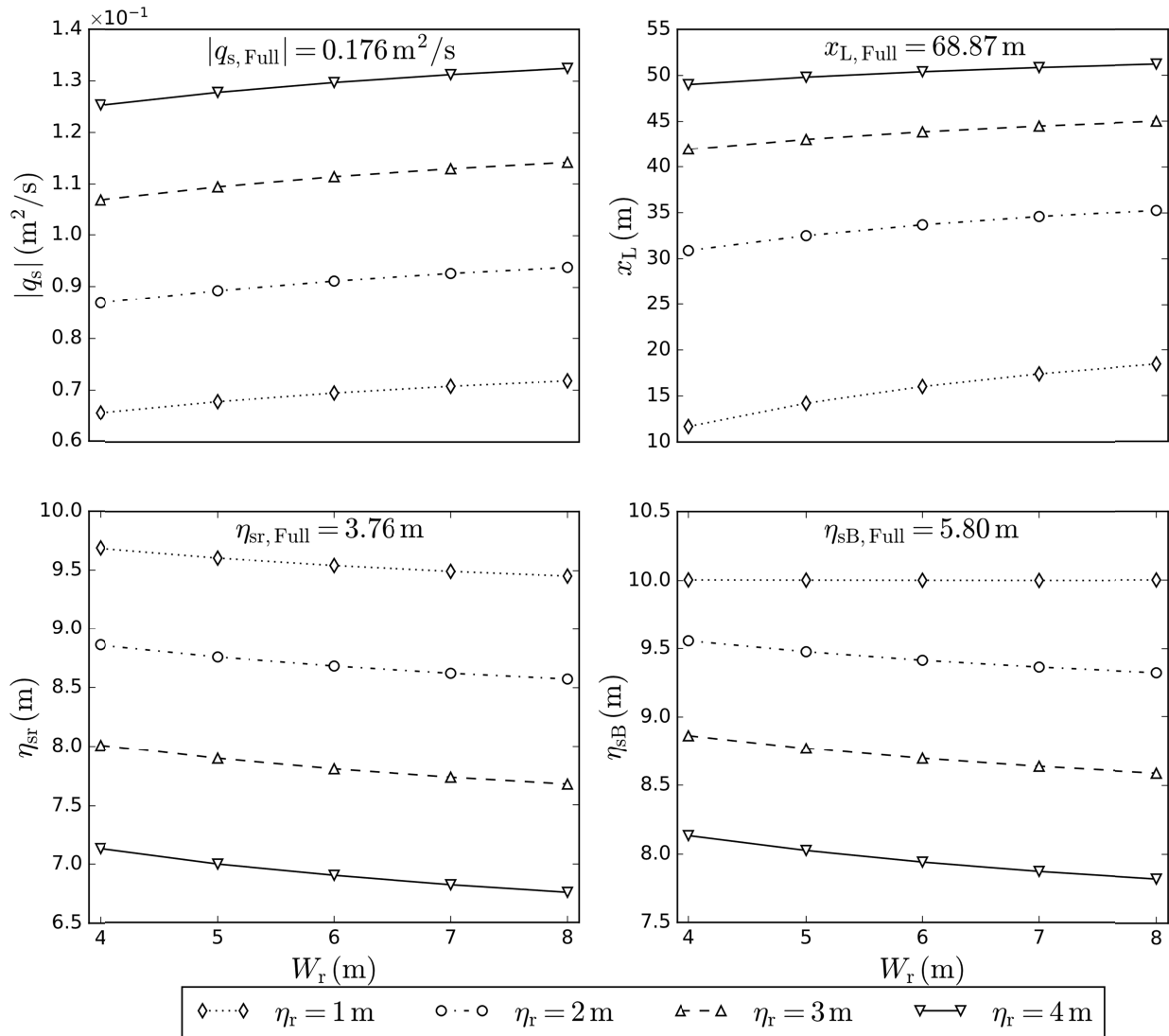
	q_s	x_L	η_{sr}
MAE	0.0151(m ² /s)	4.31 (m)	0.63 (m)
RMSE	0.0154 (m ² /s)	6.21 (m)	0.64 (m)
PBIAS (%)	13.1	9.85	-8.21
NSE	0.37	0.47	0.52

406

407 Figure 5 represents the results of sensitivity analysis using the analytical solution, in
 408 which the sensitivity of q_s , x_L , η_{sr} and η_{sB} to changes in W_r and η_r are shown. The results show
 409 that river penetration depth plays a more important role than the river width, in terms of the
 410 effect on all four output variables. Increasing η_r (i.e. depth of river penetration) from 1 to 4 m led
 411 to larger $|q_s|$ and x_L , while the values of η_{sr} and η_{sB} decreased (i.e. the depth of the lens increased),
 412 signifying larger riparian lenses next to deeper rivers, as expected. Deepening the river from 1 to
 413 4 m increased q_s by an average of 87% and x_L by an average 231%, while η_{sr} decreased by an
 414 average of 28%, and η_{sB} decreased by an average of 20%. The results also indicate that the river
 415 penetration depth has a larger effect on q_s and x_L for narrower rivers, while the river penetration
 416 depth has almost the same impact on η_{sr} and η_{sB} for different values of W_r .

417

418



419

420 **Figure 5.** Sensitivity analysis of riparian lens characteristics to river geometries. $|q_{s, Full}|$, $x_{L, Full}$,
 421 $\eta_{sr, Full}$ and $\eta_{sB, Full}$ represent the corresponding value of q_s , x_L , η_{sr} and η_{sB} for a fully penetrating
 422 river, respectively.

423

424 Figure 5 illustrates that by increasing W_r , larger q_s and x_L were obtained, while η_{sr} and η_{sB}
 425 decreased. That is, wider rivers are expected to have more extensive riparian lenses. Widening
 426 the river (increasing W_r) from 4 to 8 m increased q_s by an average of 7% and x_L was larger by an
 427 average of 21%, while η_{sr} and η_{sB} were smaller by 4% and 2%, on average. This indicates that W_r
 428 has a larger effect on q_s and x_L for shallower rivers, while the effect of W_r on η_{sr} and η_{sB} was
 429 almost independent of η_r .

430 Values of $|q_{s, Full}|$, $x_{L, Full}$, $\eta_{sr, Full}$ and $\eta_{sB, Full}$, representing a fully penetrating river, are also
 431 given in Figure 5 (formulae for fully penetrating rivers given by Werner and Laattoe (2016) and
 432 omitted here for brevity). As expected, the assumption of a fully penetrating river for situations

433 involving partially penetrating rivers may lead to significant overestimates of q_s and x_L , and
434 underestimates of η_{sr} .

435 **4 Conclusions**

436 Previous analytical models for the shape of riparian lenses in saline aquifers (adjacent to
437 gaining rivers) have presumed that the river penetrates the entire aquifer depth. However, we
438 introduce a new methodology for calculating the saltwater discharge and the shape of the riparian
439 lens adjoining a gaining river that partially penetrates an otherwise saline aquifer. The derived
440 analytical solution is solved through an iterative procedure, and is verified by comparison to
441 numerical simulation.

442 The results of the proposed analytical solution, in terms of the lens extent and saltwater
443 discharge, were in reasonable agreement with numerical modelling values. However, the
444 departure from the D-F assumption near the river for cases involving the shallowest rivers
445 introduced some errors in the lens geometry. This took the form of shorter lenses and less
446 saltwater discharge.

447 The assumption of a fully penetrating river (when the river is in reality partially
448 penetrating) leads to larger riparian lenses in both horizontal extent and vertical depth. Also,
449 fully penetrating rivers involve greater saltwater discharge compared to partially penetrating
450 rivers.

451 Differences between numerical and analytical models were, on average, 14% for
452 saltwater discharge and 13% for the lens' horizontal extent. The analytical solution tended to
453 underestimate both saltwater discharge and the horizontal extent of the lens.

454 Sensitivity analysis, based on the proposed analytical solution, shows that larger riparian
455 lenses are produced adjacent to deeper and wider rivers, as expected. The river depth is more
456 influential factor on the saltwater discharge and the horizontal extent of the lens compared to the
457 river width, for the cases that we considered. Changing the width or depth of the river had more
458 influence on the saltwater discharge and the horizontal extent of the lens for shallower and
459 narrower rivers. The proposed analytical methodology provides a useful screening tool for
460 examination of the occurrence of riparian lens in the floodplain saline aquifer adjacent to gaining
461 river of partial penetration to the aquifer.

462 **Acknowledgements**

463 The authors are thankful for helpful discussions with Hubert Morel-Seytoux (Hydroprose
464 International Consulting) regarding his analytical methodology on river-aquifer exchange fluxes
465 for partially penetrating rivers. Adrian Werner is the recipient of an Australian Research Council
466 Future Fellowship (project number FT150100403). Amir Jazayeri is funded by the Australian
467 Research Council (project numbers FT150100403 and LP140100317). Chunhui Lu
468 acknowledges the financial support from the National Key Research Project
469 (2018YFC0407200), National Natural Science Foundation of China (51679067 and 51879088),
470 and Fundamental Research Funds for the Central Universities (B200204002). The relevant data
471 arising from this research are listed in the references, tables, and figures contained herein. Any
472 additional details can be obtained from the corresponding author
473 (amir.jazayeri@flinders.edu.au).

474 **References**

- 475 Alaghmand, S., Beecham, S., Jolly, I. D., Holland, K. L., Woods, J. A., & Hassanli, A. (2014),
 476 Modelling the impacts of river stage manipulation on a complex river-floodplain system
 477 in a semi-arid region. *Environmental Modelling and Software.*, 59, 109–126.
 478 <https://doi.org/10.1016/j.envsoft.2014.05.013>
- 479 Alaghmand, S., Beecham, S., Woods, J. A., Holland, K. L., Jolly, I. D., Hassanli, A., & Nouri, H.
 480 (2015), Injection of fresh river water into a saline floodplain aquifer as a salt interception
 481 measure in a semi-arid environment. *Ecological Engineering*, 75, 308–322.
 482 <https://doi.org/10.1016/j.ecoleng.2014.11.014>
- 483 Cartwright, I., Weaver, T. R., Simmons, C. T., Fifield, L. K., Lawrence, C. R., Chisari, R., &
 484 Varley, S. (2010), Physical hydrogeology and environmental isotopes to constrain the
 485 age, origins, and stability of a low-salinity groundwater lens formed by periodic river
 486 recharge: Murray Basin, Australia. *Journal of Hydrology*, 380(1-2), 203–221.
 487 <https://doi.org/10.1016/j.jhydrol.2009.11.001>
- 488 Cendón, D. I., Larsen, J. R., Jones, B. G., Nanson, G. C., Rickleman, D., Hankin, S. I., Pueyo, J.
 489 J., & Maroulis, J. (2010), Freshwater recharge into a shallow saline groundwater system,
 490 Cooper Creek floodplain, Queensland, Australia. *Journal of Hydrology*, 392(3–4), 150–
 491 163. <https://doi.org/10.1016/j.jhydrol.2010.08.003>
- 492 Guo, W., & Langevin, C. D. (2002), *User's Guide to SEAWAT: A Computer Program For*
 493 *Simulation of Three-Dimensional Variable-Density Ground-Water Flow*, U.S. Geological
 494 Survey Techniques of Water-Resources Investigations. Book 6, Chapter A7, 77 pp.,
 495 Tallahassee, Florida.
- 496 Haitjema, H. M. (1987), Comparing a three-dimensional and a Dupuit-Forchheimer solution for
 497 a circular recharge area in a confined aquifer. *Journal of Hydrology*, 91, 83–101.
 498 [https://doi.org/10.1016/0022-1694\(87\)90130-2](https://doi.org/10.1016/0022-1694(87)90130-2)
- 499 Hantush, M. S. (1965), Wells near Streams with Semipervious Beds. *Journal of Geophysical*
 500 *Research*, 70(12), 2829–2838. <https://doi.org/10.1029/JZ070i012p02829>
- 501 Harbaugh, A. W., Banta, E. R., Hill, M. C., & McDonald, M. G. (2000), *MODFLOW-2000, the*
 502 *U. S. Geological Survey Modular Ground-Water Model - User Guide to Modularization*
 503 *Concepts and the Ground-Water Flow Process*, U. S. Geological Survey, Open File, 00-
 504 92, 121 pp., Reston, Virginia.
- 505 Holland, K. L., Charles, A. H., Jolly, I. D., Overton, I. C., Gehrig, S., & Simmons, C. T. (2009),
 506 Effectiveness of artificial watering of a semi-arid saline wetland for managing riparian
 507 vegetation health. *Hydrological Processes.*, 23(24), 3474–3484.
 508 <https://doi.org/10.1002/hyp.7451>
- 509 Laattoe, T., Werner, A. D., Woods, J. A., & Cartwright, I. (2017), Terrestrial freshwater lenses:
 510 Unexplored subterranean oases. *Journal of Hydrology*, 553, 501–507.
 511 <https://doi.org/10.1016/j.jhydrol.2017.08.014>
- 512 Langevin, C. D., Thorne Jr., D. T., Dausman, A. M., Sukop, M. C., & Guo, W. (2008), *SEAWAT*
 513 *Version 4: A Computer Program for Simulation of Multi-Species Solute and Heat*
 514 *Transport*, U. S. Geological Survey Techniques and Methods. Book 6, Chapter A22, 39
 515 pp., Reston, Virginia.

- 516 Miracapillo, C., & Morel-Seytoux, H. J. (2014), Analytical solutions for stream-aquifer flow
517 exchange under varying head asymmetry and river penetration: Comparison to numerical
518 solutions and use in regional groundwater models. *Water Resources Research*, 50(9),
519 7430–7444. <https://doi.org/10.1002/2014WR015456>
- 520 Morel-Seytoux, H. J. (1975), A Simple Case of Conjunctive Surface-Ground-Water
521 Management. *Ground Water*, 13(6), 506–515. [https://doi.org/10.1111/j.1745-](https://doi.org/10.1111/j.1745-6584.1975.tb03620.x)
522 [6584.1975.tb03620.x](https://doi.org/10.1111/j.1745-6584.1975.tb03620.x)
- 523 Morel-Seytoux, H. J. (2009), The turning factor in the estimation of stream-aquifer
524 seepage. *Ground Water*, 47(2), 205–212. [https://doi.org/10.1111/j.1745-](https://doi.org/10.1111/j.1745-6584.2008.00512.x)
525 [6584.2008.00512.x](https://doi.org/10.1111/j.1745-6584.2008.00512.x)
- 526 Morel-Seytoux, H. J., Mehl, S., & Morgado, K. (2014), Factors Influencing the Stream-Aquifer
527 Flow Exchange Coefficient. *Ground Water*, 52(5), 775–781.
528 <https://doi.org/10.1111/gwat.12112>
- 529 Morel-Seytoux, H. J., Miller, C. D., Miracapillo, C. & Mehl, S. (2017), River Seepage
530 Conductance in Large-Scale Regional Studies. *Groundwater*, 55(3), 399–407.
531 <https://doi.org/10.1111/gwat.12491>
- 532 Moriasi, D., Arnold, J., Van Liew, M., Bingner, R., Harmel, R., & Veith, T. (2007), Model
533 evaluation guidelines for systematic quantification of accuracy in watershed simulations.
534 *Transactions of the ASABE*, 50(3), 885–900. <https://doi.org/10.13031/2013.23153>
- 535 Munday, T., Fitzpatrick, A., Doble, R. C., Berens, V., Hatch, M., & Cahill, K. (2006), The
536 combined use of air, ground and 'in river' electromagnetics in defining spatial processes
537 of salinisation across ecologically important floodplain areas: Lower River Murray, SA,
538 In: Regolith 2006: Consolidation and Dispersion of Ideas, pp. 249–255, CRC LEME,
539 Hahndorf, Australia. [Available at
540 www.crcleme.org.au/Pubs/Monographs/regolith2006/Munday_T.pdf.]
- 541 Telfer, A., Burnell, R., Woods, J., & Weir, Y. (2012), River Murray floodplain salt mobilisation
542 and salinity exceedances at Morgan, prepared by Australian Water Environments for the
543 Murray-Darling Basin Authority, *MDBA Pub. No. 53/12*, 175.
- 544 Werner, A. D. (2017), Correction factor to account for dispersion in sharp-interface models of
545 terrestrial freshwater lenses and active seawater intrusion. *Advances in Water Resources*,
546 102, 45–52. <https://doi.org/10.1016/j.advwatres.2017.02.001>
- 547 Werner, A. D., & Laattoe, T. (2016), Terrestrial freshwater lenses in stable riverine settings:
548 Occurrence and controlling factors. *Water Resources Research*, 52(5), 3654–3662.
549 <https://doi.org/10.1002/2015wr018346>
- 550 Werner, A. D., Kawachi, A., & Laattoe, T. (2016), Plausibility of freshwater lenses adjacent to
551 gaining rivers: Validation by laboratory experimentation. *Water Resources Research*,
552 52(11), 8487–8499. <https://doi.org/10.1002/2016wr019400>
- 553 Zheng, C., & Wang, P. P. (1999), *MT3DMS: A modular three-dimensional multispecies*
554 *transport model for simulation of advection, dispersion and chemical reactions of*
555 *contaminants in groundwater systems: Documentation and user's guide*, Contract Report
556 SERDP-99-1, U.S. Army Corps of Engineers-Engineer Research and Development
557 Center.

558 **Notations**

559	α_L [L]	longitudinal dispersivity
560	α_T [L]	transverse dispersivity
561	η_a [L]	depth of aquifer base below the riverbed
562	η_f [L]	freshwater thickness
563	η_r [L]	river penetration depth
564	$\eta_s; \eta_{s1}; \eta_{s2}$ [L]	saltwater thickness (the depth of saltwater flow)
565	η_{sb} [-]	saltwater thickness at the landward boundary located at x_b
566	η_{sB} [L]	saltwater thickness at x_B
567	$\eta_{sB, Full}$ [L]	saltwater thickness at x_B for fully penetrating river
568	η_{sL} [L]	saltwater thickness the lens tip
569	η_{sr} [L]	saltwater thickness at the origin (adjacent to the riverbank)
570	$\eta_{sr, Full}$ [L]	saltwater thickness at the origin (adjacent to the riverbank) for fully
571		penetrating river
572	μ_f [ML ⁻¹ T ⁻¹]	freshwater dynamic viscosity
573	μ_s [ML ⁻¹ T ⁻¹]	saltwater dynamic viscosity
574	ρ_f [ML ⁻³]	freshwater density
575	ρ_s [ML ⁻³]	saltwater density
576	Γ [-]	one-side dimensionless conductance
577	Γ_c [-]	one-side dimensionless conductance in the presence of a clogging layer
578	Γ_{flat} [-]	one-side dimensionless conductance in case of no penetration of the river
579		or a flat recharge zone
580	Γ_p [L]	one-side dimensionless conductance in case of partial penetration of the
581		river
582	Γ_s [-]	modified one-side dimensionless conductance for saltwater flow
583	ΔA [L ²]	cell cross-sectional area perpendicular to the flow
584	ΔL [L]	cell size in the direction of flow
585	$\Delta x; \Delta y; \Delta z$ [L]	cell size in x , y and z directions, respectively
586	$a; b; c$ [-]	coefficients in equation (16)
587	$a_1; a_2$ [-]	coefficients in equation (24)
588	B_r [L]	clogging layer (resistive material) thickness
589	C_{GHB} [L ² T ⁻¹]	general-head boundary conductance
590	d [L]	average aquifer thickness

591	d_p^N [-]	normalised degree of penetration of the river (freshwater only)
592	d_s [L]	average thickness of saltwater between the riverbank and at distance x_B
593	d_{sp}^N [-]	saltwater normalised degree of penetration
594	D_m [L^2T^{-1}]	molecular diffusion
595	h_B [L]	head in the aquifer at x_B
596	h_r [L]	head in the river
597	h_s [L]	equivalent saltwater head
598	h_{sB} [L]	equivalent hydrostatic saltwater head at x_B
599	h_{sr} [L]	equivalent hydrostatic saltwater head at the river
600	K [LT^{-1}]	aquifer freshwater hydraulic conductivity
601	K_c [LT^{-1}]	clogging layer freshwater hydraulic conductivity
602	K_s [LT^{-1}]	saltwater hydraulic conductivity of the aquifer
603	K_{sc} [LT^{-1}]	saltwater hydraulic conductivity of the clogging layer
604	L [L]	river reach length (perpendicular to the river cross-section)
605	n [-]	effective porosity
606	q_s [L^2T^{-1}]	steady-state saline groundwater discharge
607	$q_{s, Full}$ [L^2T^{-1}]	steady-state saline groundwater discharge for fully penetrating river
608	Q [L^3T^{-1}]	fresh groundwater flow to each side of the river
609	S_y [-]	specific yield
610	S_s [L^{-1}]	specific storage
611	W_p^N [-]	normalized wetted perimeter (freshwater only)
612	W_p [L]	wetted perimeter of the river (freshwater only)
613	W_r [L]	half of the river width
614	W_{sp}^N [-]	saltwater normalised wetted perimeter
615	W_{sp} [L]	total wetted perimeter through which saltwater discharges (on both sides
616		of the river)
617	$x; x_1; x_2$ [L]	horizontal distance from riverbank
618	x_b [L]	landward boundary distance from riverbank
619	x_B [L]	“far distance” from the river where the D-F assumption is valid
620	x_L [L]	riparian lens extent
621	$x_{L, Full}$ [L]	riparian lens extent for fully penetrating river

622

623 NSE Nash-Sutcliffe efficiency

624 MAE mean absolute error

625 RMSE root mean square error

626 PBIAS percent bias